Encapsulation of RNA Molecules in BSA Microspheres and Internalization into *Trypanosoma Brucei* Parasites and Human U2OS Cancer Cells

Ulyana Shimanovich, Itai Dov Tkacz, Dror Eliaz, Artur Cavaco-Paulo, Shulamit Michaeli, and Aharon Gedanken**

RNA was encapsulated in bovine serum albumin (BSA) microspheres using a one-step sonochemical process from an water–oil solvent biphasic system. Confocal microcoscopy and fluorescence-activated cell sorting indicate that a CY3-RNA (RNA labeled with red fluorescent indocarbocyanine Cy3 dye) sphere is encapsulated in the BSA outer sphere. The diameter of the sphere depends on the number of nucleotides of the RNA, ranging from 0.63 to 2.74 μm. Total RNA (t-RNA) was used as a prototype for the future small interfering RNA (siRNA) delivery. A very broad size distribution characterizes the RNA spheres and therefore, among the loaded BSA spheres, there were sufficiently small spheres to be successfully introduced into *trypanosoma brucei* parasites and *human osteosarcoma* U2OS cancer cells.

1. Introduction

In recent years, pharmaceutical research has led to the development of several novel drug-delivery systems. Complex drug-delivery mechanisms are being developed, including the ability of the drugs to permeate the cell membranes and reach the cell cytoplasm. Micelles have attracted much attention as promising drug-delivery agents because their size and structure are similar to those of some viruses and lipoproteins that are natural carriers in biological systems.[1,2] Another advantage of micelle drug carriers arises from the specific core–shell structure of the micelles. The hydrophobic inner core surrounded by a hydrophilic outer shell forms a microcontainer that is separated from the outer environment. Therefore, the molecules entrapped in the microcontainer are protected from the outer environment.

RNA encapsulation and delivery is a new field of research that has coalesced during the past decade from independent studies on various organisms. There are many obstacles to in vivo delivery of RNA, such as degradation by enzymes in blood, interaction with blood components and non-specific uptake by the cells, which govern the biodistribution of the RNA in the body. The main goal that scientists are facing is to find a way to deliver RNA into cells and to protect RNA from degradation due to the influence of the outer environment. Since the late 1980s, scientists studying plants and fungi have known that interactions between homologous DNA and/or RNA sequences can silence genes and induce DNA methylation.[3] The gene silencing by RNA interference (RNAi) and by double-stranded RNA (dsRNA) became possible by using small-interfering RNA (siRNA) <30 bp in mammalian cells;[4,5] siRNA and dsRNA have become the tool for gene function studies.[6–11] However, owing to its relatively large size and anionic charge, one of the key problems in utilizing siRNA as a therapeutic tool is the availability of effective delivery systems.[11] A number of approaches for delivering siRNA have been explored recently.[12–15] Examples of these systems include polymer-based microparticules, micelles, and liposomes.

In the present work, ultrasonic waves were used for the formation of proteinaceous microspheres (PMs) and RNA encapsulation in the PMs. The role of PMs is to protect RNA from the outer environment and to control time and rate of RNA release. For the encapsulation studies, a total RNA (t-RNA) was used as a prototype for siRNA delivery. Micrometer-sized gas- or liquid-filled microspheres could be produced for various kinds of proteins, such as bovine serum albumin (BSA),[16–18] human serum albumin (HAS),[19] and hemoglobin (Hb),[20] by using an ultrasonic emulsification method. Moreover, we have recently shown that PMs could be produced from a mixture of two kinds of protein.[21] The mechanism of the sonochemical formation of microspheres has been discussed previously.[22–25] According to the mechanism of the sonochemical formation of PMs, the microspheres are formed by chemically crosslinking cysteine residues of the protein, which undergo oxidation by a $HO_2\cdot$ radical formed inside or around a micrometer-sized

U. Shimanovich, Prof. A. Gedanken
Department of Chemistry and Kanbar Laboratory for Nanomaterials
Bar-Ilan University Center for Advanced Materials and Nanotechnology
Bar-Ilan University
Ramat-Gan 52900, Israel
E-mail: ushimanovich@yahoo.com; gedanken@mail.biu.ac.il
Dr. I. D. Tkacz, D. Eliaz, Prof. S. Michaeli
Mina and Everard Goodman Faculty of Life Sciences
Bar-Ilan University
Ramat-Gan, 52900, Israel
Prof. A. Cavaco-Paulo
University of Minho
Textile Engineering Department
P-4800058 Guimaraes, Portugal

DOI: 10.1002/adfm.201100963

gas bubble or a non-aqueous droplet. The formation of S–S bonds is the chemical crosslinking process that is responsible for the formation of the microspheres, and is a direct result of the chemical effects of ultrasound radiation on an aqueous medium. We have also demonstrated that, if a drug, e.g., Tetracycline,[26] Taxol,[27] and Gemzar,[28] is present in the precursor mixture for the preparation of PMs, it is encapsulated in the PM. Proteases released the drug in a fast release mode and its activity was measured.

The creation of BSA microspheres and the encapsulation of RNA in the spheres were achieved by a one-step process, starting with the native BSA protein, dodecane or oil (soya bean oil, canola oil, or olive oil) and RNA. Total RNA was used for the initial studies of RNA encapsulation, it was followed later by employing other types of RNA. We have previously reported sonochemical synthesis of RNA[29] and DNA nanospheres[30] and their introduction into mammalian cancer cells. The idea of the current research is to find the method to protect RNA molecules by encapsulating it in a protein scaffold.

The main objective of this research was to study the efficiency of the sonochemical method for RNA encapsulation in PMs, and to study the possibility of using PMs as a drug-delivery agent to *trypanosoma brucei* (*T.b.*) parasites and to mammalian cells (human U2OS cancer cells). Trypanosomes are parasitic protozoans that include several medically and a variety of economically important parasites, such as *T.b.*, the causative agent of sleeping sickness. Trypanosomatids poses and active RNAi machinery. Unlike mammalian cells, endocytosis and exocytosis is mediated via a 100 nm flagella pocket. The flagella pocket is responsible for the entry of nanovehicles and RNA delivery into the body of the cell. Currently, new drugs to treat trypanosomas are under demand, and siRNAs are such potential novel drugs. The *human osteosarcoma* U2OS cell line is one of the first generated cell lines and is used in various areas of biomedical research. It was in our interest to demonstrate the possibility of spontaneous internalization and RNA delivery into two different types of cells: parasites (host cells) and cancer human cells.

2. Results and Discussion

The efficiency of the sonochemical method in encapsulating RNA within PMs was studied using spectrophotometric analysis. The amount of RNA loaded was assayed using a NanoDrop 1000 spectrophotometer at 260 nm. The amount of RNA loaded in the BSA microspheres was determined by subtracting the amount of RNA in the residual microsphere phase (the lower phase in the separation flask) from its total amount in the precursor solution. For the initial studies t-RNA was used as a phenotype of siRNA. About ≈40% of the t-RNA was found in the residual microsphere phase, which means that ≈60% was encapsulated in the BSA microspheres. No residue of t-RNA was found in the excess dodecane (the upper phase). To reinsure the results (percentage of loaded t-RNA) and to check if during the sonication process the t-RNA was damaged or not, a "primer extinction" method was used. This method is based on the identification of the number of bases and their sequence in the RNA. The percentage loading results were quite similar to

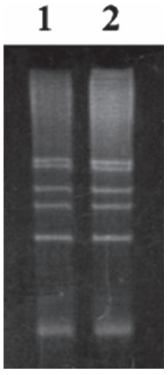

Figure 1. 1) RNA elution from PMs, 2) RNA elution from the lower phase of the PMs (RNA molecules that were not encapsulated within PMs). The ratio between the amount of RNA outside the spheres and inside the spheres is 1:1.2, which means that about 56% of the RNA was encapsulated inside the microspheres.

results obtained by using spectrophotometric analysis. **Figure 1** presents the results of the application of the primer extension technique to RNA loaded in BSA spheres. About ≈56% of t-RNA was found to be encapsulated in the BSA microspheres. The obtained t-RNA band proves that during sonochemical microspherization, the encapsulated RNA was not damaged.

The lower value of encapsulated t-RNA (4% difference from the spectroscopic method) obtained using the "primer extension" technique (56% vs. 60% by the spectrophotometric analysis) could be explained by the destruction of the PMs during t-RNA elution.

The influence of different organic solvents on the efficiency of RNA encapsulation was checked. The results are presented in **Table 1**. The results indicate that with an increase in the viscosity and density of the organic solvent, the percentage of encapsulated RNA decreased. Moreover, the biocompatibility of the organic solvents used in the current experiments was checked, and the soya-bean oil was found to be the most biocompatible organic solvent for *T.b.* parasites and U2OS cells. The biocompatibility of organic solvents for parasites and cancer cells was studied by following (using light microscopy) changes in the morphology and life times of the parasites and cells. Soya bean oil does not cause any damage, neither to parasites nor to cells. It is well documented that the formation of the acoustic bubble is strongly dependent on the viscosity of the solvent. The correlation between the yield of the PM formation and the organic solvent viscosity is just another demonstration of this dependence. In addition, the size dependence of the RNA encapsulated in BSA spheres was studied as a function

Table 1. Dependence of the PM formation yield on the viscosity of the organic over layering solvent.

	Dodecane	Canola oil	Soya oil	Olive oil
Viscosity [cP=mPa.s]	13,4	57	69	81
Density g cm^{-3}	0.7493	0.92	0.92	1.0
% encapsulated RNA within BSA spheres	65	47	43	31

Table 2. Size dependence of the RNA encapsulated in BSA spheres as a function of the number of nucleotides in the RNA chain. The size of the spheres was determined by dynamic light scattering (DLS) measurements.

RNA type	RNA length [number of nucleotides]	Size of RNA-loaded PMs [μm]
t-RNA (total RNA)	≈8000	2,74
T.b. RNA	200	1.6
S.L.RNA (Splice Leader RNA)	180	1.5
Colosoma-RNA	95	0.8
CY3 oligo RNA	40	0.63

of the number of nucleotides in the RNA chain. The change in size was studied using dynamic light scattering, and the results are presented in **Table 2**. The results show that the size of the microsphere (BSA microsphere with RNA inside) increases with an increase of the number of nucleotides in the RNA chain.

In order to understand the amount (in%) of RNA encapsulated in BSA spheres versus the type of organic solvent, the "coloring test" was performed. The dodecane made, unloaded and loaded (with t-RNA) BSA spheres, were colored with Nile Red dye, as described in the Experimental Section and analyzed by fluorescence-activated cell sorting (FACS; a specialized type of flow cytometry). It provides a method for sorting a heterogeneous mixture of microspheres into two or more containers, one group of spheres at a time, based upon the specific light scattering and fluorescence characteristics of each group of spheres. It is a useful scientific technique as it provides a fast, objective, and quantitative recording of fluorescent signals from individual microsphere as well as the physical separation of spheres of particular interest. Nile Red is a dye with a solvent-dependent absorption spectrum. It is an uncharged hydrophobic molecule whose fluorescence is strongly influenced by the polarity of its environment. With an increase in the polarity of the environment, the maximum of emission shifts to a shorter wavelength (from about 650 in water to 470 in oil).[31] The dye is photostable and the working wavelength range is broad and removed from wavelengths at which many biomolecules absorb. The fluorescence of Nile Red is unaffected in the pH range between 4.5 and 8.5.[32] Nile Red is widely used to detect the hydrophobicity/hydrophylicity of the environment. The results of FACS measurements are also presented in **Figure 2**. The changes in size between RNA-loaded PMs and unloaded-PMs are detected by

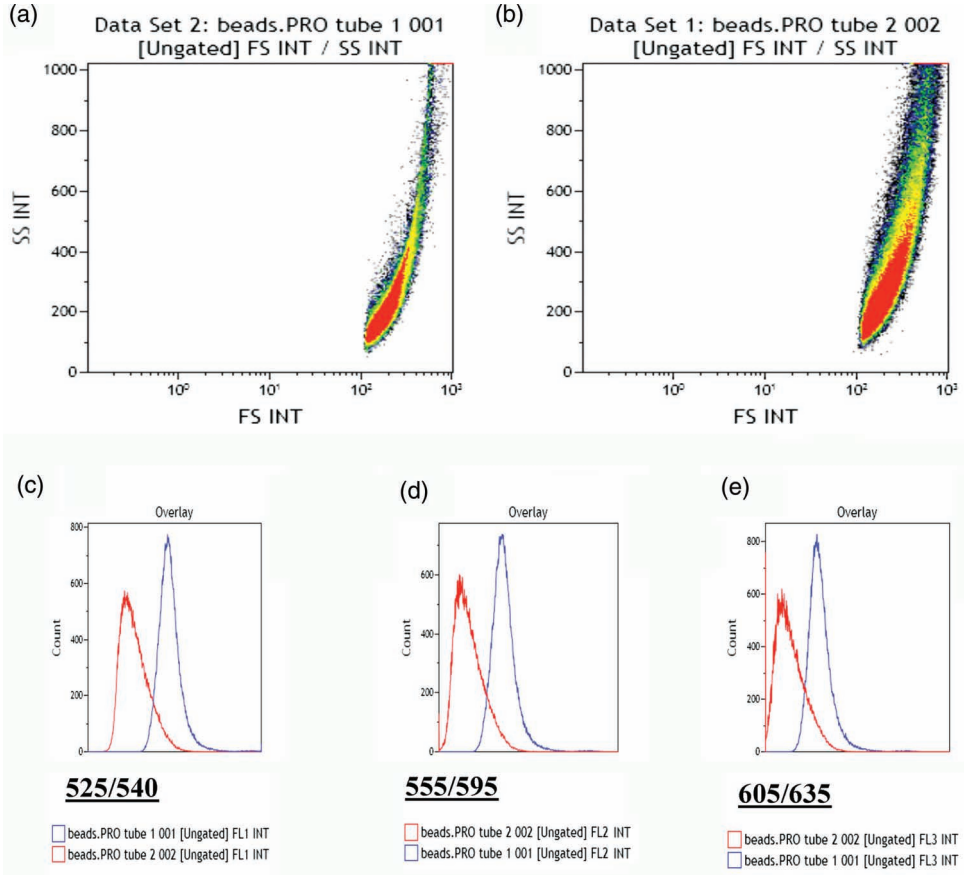

Figure 2. Flow cytometry analysis of a mixture of microspheres. a) Size distribution of BSA microspheres with an average size of about 1.6 μm. b) Size distribution of t-RNA-loaded BSA microspheres with an average size of 2.7 μm. c) Overlaid histograms of the fluorescence of BSA microspheres (red line) with an emission peak at 525 nm and t-RNA-loaded BSA microspheres (blue line) with an emission peak at 540 nm. d) The fluorescence of BSA microspheres (red line) with emission peak at 555 nm and t-RNA-loaded BSA microspheres (blue line) with an emission peak at 595 nm. e) The fluorescence of BSA microspheres (red line) with an emission peak at 605 and t-RNA-loaded BSA microspheres (blue line) with an emission peak at 635 nm. For all fluorimetric measurements (a–c) excitation was measured at 488 nm. Before fluorimetric measurements, samples were washed twice with double-distilled water.

FACS and presented in Figure 2a and b. Figure 2a represent the size distribution of the BSA spheres with average size of 1.6 µm. Figure 2b represent the size distribution of t-RNA-loaded PMs with an average size of 2.7 µm.

The fluorimetric measurements of BSA spheres and t-RNA-loaded BSA spheres are presented in Figure 2c–e. When a pristine BSA protein was microspheridized, the fluorescence spectra of Nile Red showed emission peaks at 525 nm, 555 nm and 605 nm (Figure 2c–e, red line). When the t-RNA was encapsulated within BSA spheres, the environment in the inner part of the BSA spheres slightly changed to be more hydrophilic. The increase in hydrophilicity of the inner part of PM results in a red shift of the fluorescent signal that emits from the inner part of the RNA loaded sphere. The change in the environment resulted in changes in the fluorescence spectra (red shift) with emission peaks at 540, 595, and 635 nm (Figure 2c–e, blue line). The changes in the intensity of the fluorescence could be explained as a result of the bonding of Nile Red molecules to the RNA. The quantity of the molecules (BSA, t-RNA, water and dodecane) in the sample of t-RNA-loaded BSA spheres is much higher than that of BSA molecules in the pristine BSA spheres. More Nile Red molecules are bonded in the case of RNA-loaded spheres.

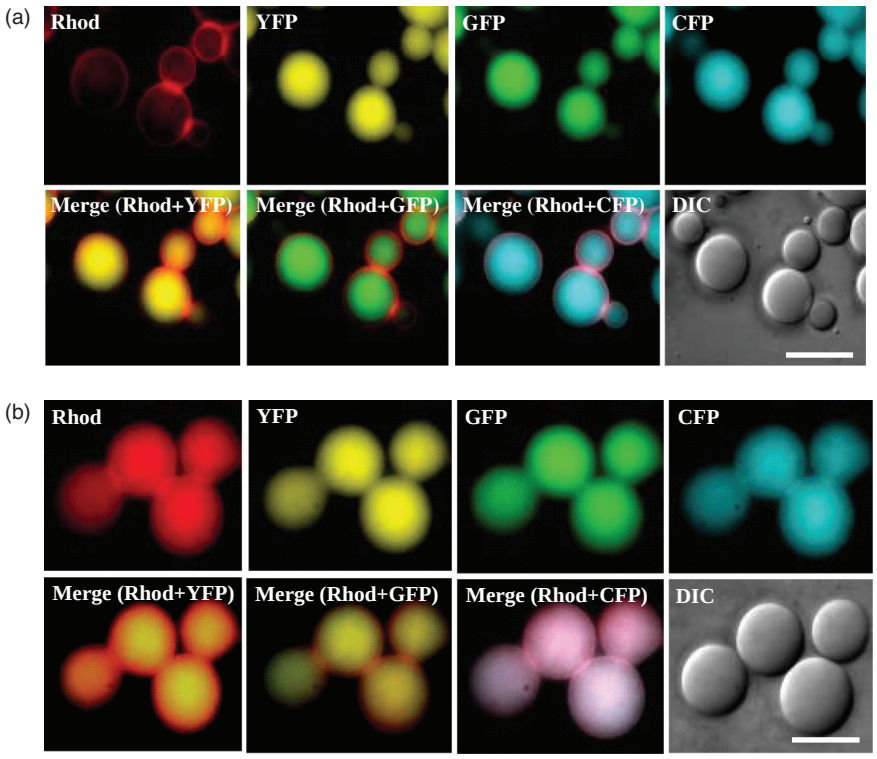

Figure 3. a) Fluorescent microscopy image of dodecane-filled BSA microspheres colored with Nile Red dye. b) Fluorescent microscopy image of dodecane-filled RNA-loaded BSA spheres colored with Nile Red dye using a Rhod. filter = red fluorescent signal (excitation at 550 nm, emission at 573 nm); YFP filter = yellow fluorescent signal (excitation at 514 nm; emission at 527 nm); GFP filter = green fluorescent signal (excitation at 489 nm; emission at 509 nm); CFP filter = blue fluorescent signal (excitation at 435 nm; emission at 476 nm). The merged figures represent the fluorescence data obtained when two fluorescent filters are used. Scale Bare = 2 µm.

The results of fluorimetric FACS measurements were confirmed by fluorescent microscopy analysis. Two samples (BSA spheres and RNA-loaded BSA spheres) were analyzed using an Apo-Tome fluorescent microscope. The following microscope fluorescent filters were used for the current analysis: Rhod (excitation 550 nm, emission 573 nm), YFP (excitation 514 nm, emission 527 nm), GFP (excitation 489 nm, emission 509 nm) and CFP (excitation 435 nm, emission 476 nm). **Figure 3**a shows fluorescent images of BSA spheres colored with Nile Red dye. The red fluorescence of the BSA spheres emanates from the shell of the spheres and the yellow, green, and blue florescent signals emanate from the inner part of the spheres. The fluorescence with longer a wavelength (red fluorescence) indicates a more hydrophilic environment. The yellow, green, and blue fluorescent signals with emissions at shorter (compared to red) wavelengths, indicate a more hydrophobic environment. It is clearly observed in Figure 3a that the nature of the BSA sphere shell is more hydrophilic (has a red fluorescent signal) than the inner part of the sphere, which is more hydrophobic (with the yellow, green, and blue fluorescent signals). When the RNA was encapsulated within the BSA spheres the hydrophobicity of the environment of the inner part of the sphere changed significantly to be less hydrophobic. The decrease in the hydrophobicity of RNA-loaded BSA spheres is depicted in Figure 3b. The red fluorescent signal of the RNA-loaded BSA spheres emanates from the shell and from the inner part of the spheres, indicating that the environment became less hydrophobic due to the RNA molecules encapsulated within the BSA spheres.

The results obtained for soya-bean oil-filled BSA spheres and RNA loaded BSA spheres are identical to dodecane filled spheres. The dodecane filled spheres were chosen to be presented in Figure 3 due to better resolution and stronger fluorescent signal.

The increase in the hydrophilicity of the inner volume of the loaded BSA spheres points out to the successful encapsulation of the RNA molecules inside the BSA spheres. The morphology of PMs and the localization of RNA molecules inside the BSA spheres were studied using confocal microscopy. CY3-RNA was used for those studies. CY3 is a reactive fluorescent marker with an excitation wavelength of 554 nm and an emission at 566 nm. CY3(red)-RNA were encapsulated inside the BSA fluorescein isothiocyanate conjugate, Fitc(green)-BSA. The results of the confocal microscopy analysis are presented in **Figure 4**. After sonication, we could identify two different kinds of microspheres synthesized sonochemically: 1) the major product exhibited a red RNA sphere (proof of its spherical structure is depicted in the 3D image) located inside a surrounding green BSA sphere; 2) mixed microspheres, where red RNA and green BSA construct the walls of the sphere. Figure 4a presents the

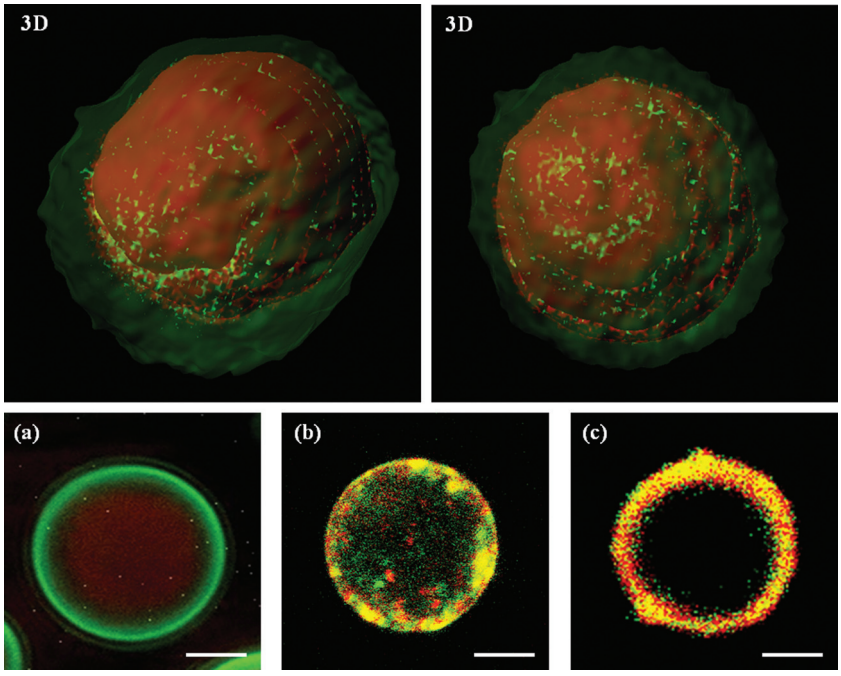

Figure 4. Confocal microscopy images of CY3-RNA (red) encapsulated within fitc-BSA (green). a) *z*-stack confocal image of PMs,where the red CY3-RNA was encapsulated inside green Fitc-BSA. b) *z*-stack confocal image of PMs with CY3-RNA after 24–25 h (the encapsulated RNA, which was found previously to be spread inside the BSA sphere is now delocalized close to the walls of the sphere). c) *z*-stack confocal image of a mixed sphere (CY3-RNA and fitc-BSA construct the walls of PM). On the upper part of the image the reconstruction of the 3D structure of PM with encapsulated CY3-RNA is presented. Left image = view from the side; right image = view from the front. The reconstruction was done from *z*-stack confocal images using "Imaris" image analysis software. Scale bar = 0.5 µm.

z-stack confocal image of PMs illustrating the red CY3-RNA encapsulated inside green Fitc-BSA. Moreover, after 24–25 h the encapsulated RNA sphere, which was found previously to be located inside the BSA sphere, is now delocalized and is found closer to the walls of the sphere (see Figure 4b). An example of the mixed sphere is depicted in Figure 4c. In addition, Figure 4 also presents the reconstruction of the 3D structure of the green BSA sphere with red RNA spheres inside. The sonochemical formation of RNA spheres is now reported.[29] The reconstruction (reconstruction of *z*-stack confocal images) was done using the "Imaris" image analysis software.[33] The green and red fluorescent signals are emitted from the walls of the sphere. This result indicates that the wall of the sphere was formed by the simultaneous contribution of red RNA and green BSA to the construction of the walls. Moreover, when the 3D image of the sphere was reconstructed, the weak green signal emitted from the inner part of the sphere was recognized, which points out to the presence of fitc-BSA in the inner part of the sphere.

Since both RNA and BSA form spheres, the question why the RNA is encapsulated in the BSA and not the reverse can be explained as follows: 1) kinetically the formation of RNA spheres is faster; 2) the ratio of BSA: RNA is so large that their interaction leads first to the formation of the BSA outer sphere carrying the RNA inside. The morphology of the loaded- and unloaded-PMs in the solution was also determined by using scanning electron microscopy (SEM). No difference is found in the morphology of the loaded- and unloaded-PMs; both depicted spherical structures. **Figure 5** presents a SEM image of the *T.b* RNA-loaded BSA spheres that were fabricated sonochemically. The spheres, shown in Figure 5, have an average size of 1.63 µm.

The size of the RNA-loaded PMs in the solution was also measured using a dynamic light scattering (DLS) apparatus. After the sonochemical emulsification, a polydispersed solution was obtained. The average size of unloaded PMs was found to be 2.5 µm (for dodecane-filled BSA spheres). The size of the loaded PMs increases with the increase in the length of encapsulated RNA molecules (Figure 5). On the other hand, the electrical charge of loaded PMs does not differ from unloaded PMs, and was found to be about –40 meV.

The above presented results substantiate our explanation that the RNA spheres are formed first and determine the size of the complex RNA-BSA sphere.

The results of the SEM measurements and statistic calculations of the size distribution of the spheres (Figure 5) are in a good agreement with the DLS data. The loaded PMs were found to be stable for about 5 months (+4 °C). The solution was checked every week and each time the presence of the spheres in the solution was checked by light microscopy. The number of spheres that remain untouched were obtained from statistic calculations using the "Scion" program.[34] The results of the calculations for the stability of the RNA-loaded PMs (the number of BSA spheres that remain stable in solution versus time) are as follows: after 1 week, about 2.3 ± 0.5% of BSA spheres were destroyed; after 1 month, 10 ± 0.5%; after 2 months, 20 ± 0.5%; after 3 months, 47 ± 0.5%; and after 5 months, 100% of the t-RNA-loaded BSA spheres were destroyed (no microspheres were found in the solution). Moreover, the results were confirmed by UV spectroscopy. Each time (every week) the absorption of a free BSA protein (at 280 nm) in the lower part of the solution was measured. The measured value was then subtracted from the initial amount of protein. The stability, size, and zeta-potential changes of t-RNA-loaded spheres at different pH values was checked using the DLS apparatus equipped with a multipurpose titration device (MPT2). To reach an acidic environment, a 0.1 M aqueous solution of HCL was titrated to the t-RNA-loaded BSA spheres and to the unloaded BSA spheres. To reach the basic environment, 0.1 M aqueous solution of NaOH was titrated to the t-RNA-loaded BSA microspheres and to unloaded BSA spheres. Two samples were compared: a) BSA spheres and b) t-RNA-loaded BSA spheres. The results of the titration test are presented in **Figure 6**. With an increase in pH values the electrical charge of BSA spheres and t-RNA-loaded BSA spheres decreases (from positive values to negative values). The average size of both types of PMs (loaded and unloaded t-RNA) changes dramatically when the pH was decreased to

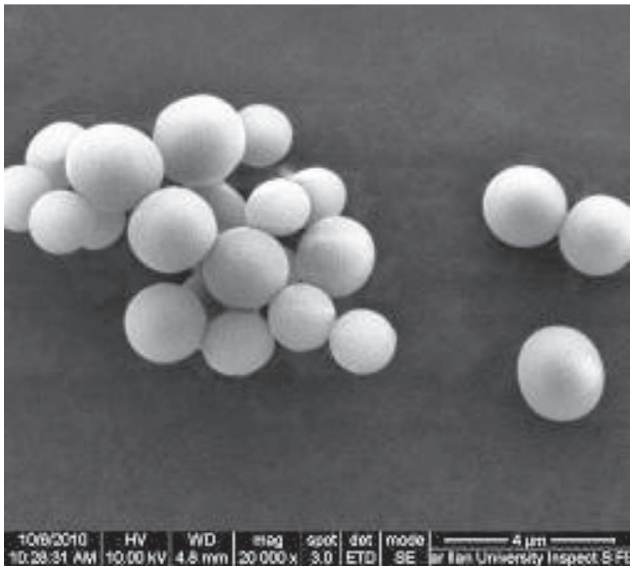

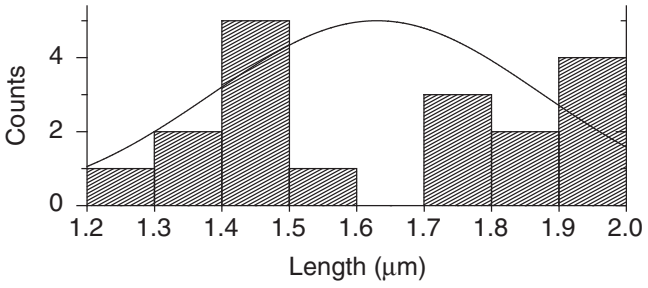

Figure 5. SEM image of *T.b.* RNA-loaded BSA microspheres. A histogram of statistic calculations of the size of *T.b.* RNA-loaded BSA spheres is presented underneath the image. The statistic calculations were done using the "Scion" program. The average size of *T.b.* RNA-loaded BSA spheres is about 1.6 µm.

under 6, meaning that at very acidic pH, PMs tend to degrade. Both types of PMs are completely destroyed at a pH below 3.

The percentage of RNA released from the inner part of the PMs versus time was checked by measuring the UV absorption of RNA at 260 nm (using a NanoDrop 1000 spectrophotometer). BSA does not absorb at this wavelength. The amount of RNA was measured for the aqueous lower phase, where only the residues of free protein and RNA molecules are presented. The results indicate that after 1 week about 2% of RNA was released; after 1 month, 11%; after 2 months 21%; after 3 months, 47%; and after 5 months 100% of the RNA was found in the aqueous phase and the microspheres were completely destroyed.

The transfer of RNA into non-viral cells is a complicated procedure because it involves the use of different mediators. In the current study, RNA (encapsulated within BSA) was successfully introduced into human U2OS cancer cells and *T.b.* parasites without any additional agents. Small RNA-loaded PMs spontaneously penetrated parasites and human cells due to the presence of small size PMs. First, the influence of the parasite and cancer cell medium on the stability of RNA-loaded spheres was checked. The medium of the parasites, as well as the medium where the cancer cells were grown, have no influence on the stability of the RNA-loaded BSA spheres. We could follow the existence of the spheres in these media by light microscopy for 24 hours. The spheres were found to be stable in both media environments. The parasites and cancer cells with the PMs were analyzed and characterized by fluorescent microscopy. The nucleus of the cancer cells as well as *T.b.* parasites was colored with a DAPI marker, which gives a blue fluorescent signal (excitation was measured at 359 nm and emission was measured at 457nm). The fluorescence collected from the cancer cells and the *T.b.* parasites passed through three filters, each filtering a different wavelength region. The filters were DIC (light microscopy), DAPI (excitation at 359 nm; emission at 457 nm) and GFP (excitation at 489; emission at 509 nm). **Figure 7** is a combination of the images of the *T.b.* parasites (and the cancer cells) when all three filters are employed. Thus, any green fluorescence is related to the presence of Fitc-BSA. The blue fluorescence originates from DAPI, a dye known to be found in the nucleus. Figure 7 shows clearly PMs (green) inside the parasites (Figure 7a) and inside the human U2OS cancer

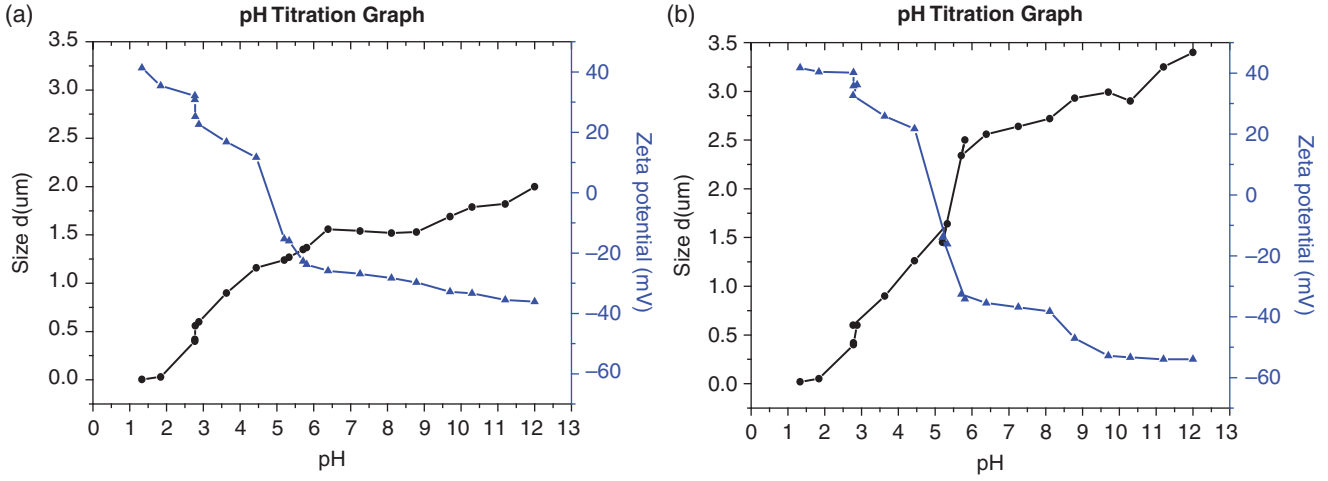

Figure 6. DLS measurement of average size distribution (µm) and zeta-potential (mV) changes at different pH values: a) BSA microspheres, b) t-RNA-loaded BSA microspheres.

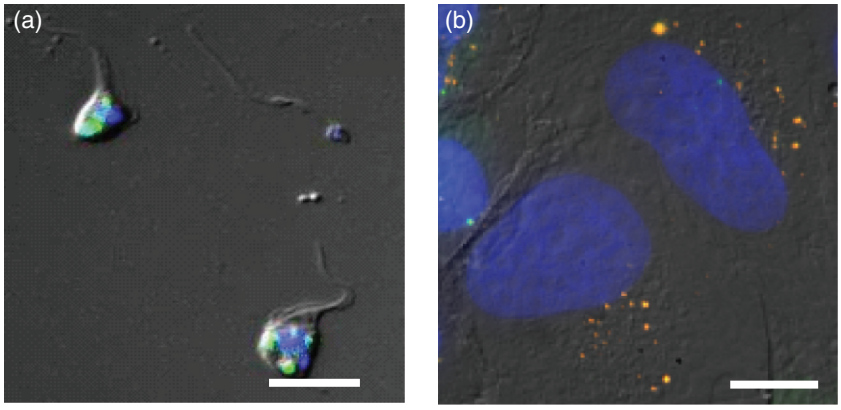

Figure 7. Fluorescent microscopy images of *T.b.* parasites with PMs as well as human U2OS cancer cells with PMs. a) Combination of the fluorescence originating from PMs (RNA-loaded PMs) entering trypanosome brucei parasites. The image combines light passing through DIC, DAPI and GFP filters. b) Fluorescence of PMs (RNA-loaded PMs) which entered human U2OS cancer cells using only DAPI, Rhod and GFP filters. Scale bar = 5 μm.

cells (Figure 7b). We could see that very few PMs entered the nucleus (see for example the green point in Figure 7b)

The estimated size of the spheres that were able to penetrate the *T.b.* parasite is about 150 nm and the sphere size, which found to be able to penetrate the cancer cells, can reach 400–500 nm. The relative size of *T.b.* parasites and U2OS cancer cells are about 5 μm and 20 μm, respectively.

3. Conclusions

In the current research we demonstrate a novel environmentally friendly method for the synthesis of RNA-loaded PMs involving the use of ultrasonic waves. The RNA-loaded spheres were used as a drug (RNA) delivery agent. For the initial studies, t-RNA was used as a phenotype for siRNA encapsulation within BSA spheres. The formation of the microspheres and RNA encapsulation was achieved by a one-step reaction. The resulted solution is a polydispersed solution of RNA-loaded BSA spheres with an average size that ranges from 0.5 μm to 2.5 μm, dependent on the length of the RNA chain. The RNA-loaded spheres were spontaneously introduced into *T.b.* parasites and human U2OS cancer cells without use of any additional mediators. The uptake of the negatively charged RNA-loaded BSA spheres by cancer cells and parasites happened due to the existence of sufficiently small spheres. In further work, we plan to explore the above-described method for siRNA encapsulation and delivery.

4. Experimental Section

Sonochemical Preparation of RNA-Loaded BSA Microspheres: The following RNA molecules were encapsulated inside the BSA spheres: 1) t-RNA, 2) SL RNA, 3) *Colosoma* RNA, 4) *T.b.* RNA, and 5) CY3-RNA. The first four types of RNA were extracted from *Lepomonas collosoma* cells using a Tizol reagent (Sigma–Aldrich). CY3-RNA was purchased from Synthessa Bioscience. The creation of the RNA-loaded microspheres was repeated by using a different concentration of RNA in the precursor solution. The preparation of t-RNA-loaded BSA microspheres followed the typical synthesis of PMs, as described previously.[21] In brief, 6.7 mL of an organic solvent (dodecane (98.0% Fluka) or soya bean oil, canola oil, or olive oil) was layered over a 10 mL water solution of a 5% w/v BSA protein (bovine serum albumin protein, Sigma–Aldrich) and 1% w/v purified t-RNA. The volume ratio between the 5% (w/v) BSA aqueous solution and dodecane was kept constant at 3:2, respectively. The molar ratio between the BSA protein and RNA was 1:50 (w/w), respectively. t-RNA-loaded PMs were synthesized with a high-intensity ultrasonic probe (Sonic and Materials, VC-600, 20 kHz, 0.5 in. a Ti horn, at 30% amplitude). The volume of the acoustic chamber was 25 mL and the total volume of all the ingredients was 16.7 mL. The bottom of the high-intensity ultrasonic horn was positioned at the aqueous-organic interface, employing an acoustic power of ≈ 45 W cm^{-2} with an initial temperature of 22 °C in the reaction cell. The sonication lasted for 3 min at 22 °C using an ice-cooling bath to maintain the low temperature. A separation flask was used to separate the product from the mother solution. The separation was accomplished within a few minutes due to the lower density of the microspheres, relative to the density of water. To obtain a more complete separation of the proteinaceous microspheres from the mother solution, the separation flasks were placed in a refrigerator (4 °C) for 24 h. After the separation, the residual aqueous phase and the organic solvent (dodecane) were removed and the product was resuspended in water. The resulted microsphere solution was washed with doubly distilled water three times.

Coloring Test: For a "coloring test", Nile Red dye (Sigma–Aldrich) was used. The dye was added to the precursor mixture (1 μg mL^{-1}) of two reactions, the microspherization of pristine BSA and the encapsulation mixture of t-RNA and BSA spheres. The resulting emulsions were than compared by using FACS (Calibur flow cytometer) and fluorescent microscopy.

Assessment of Quality Encapsulated RNA Inside BSA Microspheres – the Extraction of RNA from BSA Spheres: The encapsulated RNA molecules were regenerated from the BSA spheres using a phenol:chloroform extraction method and further precipitated with ethanol according to the manufacture's instructions. The quality of the extracted RNA was assessed by a primer extension technique and compared to the untreated RNA.

Determination of RNA Concentration in the BSA Microspheres: The amount of RNA loaded in the microspheres was determined by using two methods: 1) Spectrophotometry, (NanoDrop 1000 UV-spectrophotometer; RNA absorption peak was measured at 260 nm) by subtracting the amount of RNA remaining in the aqueous solution after the sonication from the initial amount of RNA, and 2) the primer extinction method (t-RNA band was measured at 95 kDa).

Determination of RNA Localization in BSA Spheres: For determining the localization of the RNA in the BSA spheres, CY3-labeled RNA was used. The encapsulation of CY3-RNA was done according to the above-described procedure. The samples were analyzed using confocal microscopy (Confocal Zeiss microscope), and 3D images were reconstructed from *z*-stack confocal cuts using the "Imaris" image analysis program (Bitplane, Switzerland).

Introduction of RNA-Loaded PMs into T.b. Prasites and Human Cells: In order to introduce the RNA-loaded PMs into *T.b.* parasites and human U2OS cancer cells, a colored BSA protein and colored RNA were used. Colored PMs were prepared by using Fitc-BSA (a fluorescein-isothiocyanate-labeled bovine serum albumin protein; Sigma–Aldrich), and CY3-labeled RNA. Soya-bean oil was used as the organic liquid for the preparation of the PMs. Fitc-BSA has a green color with an excitation peak at 488 nm and an emission peak at 520 nm. To follow the RNA encapsulation, red CY3-RNA was used (its excitation peak was measured at 650 nm, and its emission peak was measured at 670 nm). *T.b.* parasites were maintained in a BACK medium. The parasites were incubated with PMs for 3 h at 37 °C. After the incubation the parasites were washed three times with a PBS×1 buffer solution in order to remove the residual PMs. The nuclei were

counterstained with DAPI. The parasites were crosslinked on a glass slide with 4% paraformaldehyde and then microscopically analyzed. Human U2OS cells were maintained in low glucose DMEM (Biological Industries, Kibbutz Beit Haemek, Israel) containing 10% fetal bovine serum (Hy-Clone Laboratories, Logan, UT). The cells were grown on a glass slide for 24 h. PMs were added to the cells and incubated for 24 h at 37 °C. After the incubation, the cells were washed five times with a PBS×1 buffer in order to remove the PMs that did not penetrate the cells. The cells were crosslinked with 4% paraformaldehyde. The nuclei were counterstained with DAPI, and coverslips were mounted in a mounting medium. The samples were analyzed using wide-field fluorescent microscopy. 3D images were reconstructed using the "Imaris" image analysis program.

Instrumentation: DLS measurements and *z*-potential measurements were carried out on an ALV/CGS-3 compact goniometer system equipped with an ALV/LSE-5003 light-scattering electronic and multipurpose titrator (MPT2), a multiple digital correlator, and a 632.8 nm JDSU laser 1145P. DLS and *z*-potential experiments were carried out in a doubly diluted, as-separated PM solution, i.e., the PMs removed after the sonication were diluted with an equal amount of doubly distilled water (DDW). Each measurement took 10 s; particle distribution and electrical charge distribution were obtained by averaging ten DLS measurements. For light microscopy (Apo-Tome microscope, Zeiss), samples were prepared by depositing the aqueous dispersions, without further purification, onto a glass slide. The RNA-loaded BSA microspheres were analyzed and characterized by SEM (JSM-840, JEOL), light microscopy (Apo-Tome microscope, Zeiss), and DLS measurements. Wide-field fluorescence images were obtained using the cell-R system based on an NIKON 90i fully motorized inverted microscope (60× Plan Apo objective, 1.42 numerical aperture [NA]) fitted with an Orca-AG charge-coupled device camera (Hamamatsu, Bridgewater, NJ), rapid wavelength switching, and driven by the cell-R software. A 3D volume of the cell containing NPs (135z-slices of 0.30 μm; total height, 40 μm) was imaged and reconstructed using the "Imaris" image analysis software. FACS measurements were conducted using a FACS Calibur flow cytometer (Becton-Dickinson) equipped with a 488-nm argon laser; results and data acquisition were analyzed using the CellQuest software[35] and a Power Macintosh G4. Samples were washed three times with doubly distilled water before each measurement.

Acknowledgements

U.S. thanks the Ministry of Science and Technology, Israel for the "Woman in science" scholarship (3-8219). We thank Dr. Yaron Shav-Tal (Bar-Ilan University, Israel) for providing U2OS cells to perform in situ experiments.

Received: February 5, 2011
Published online: August 9, 2011

[1] K. Kataoka, G. Kwon, M. Yokoyama, T. Okano, Y. Sakurai, *J. Controlled Release* **1993**, *24*, 119–132.
[2] Z. Rahman, A. S. Zidan, M. J. Habib, M. A. Khan, *Eur. J. Pharm. Biopharm.* **2011**, *77*, 26–35.
[3] M. Fagard, H. Vaucheret, *Annu. Rev. Plant Physiol. Plant Mol. Biol.* **2000**, *51*, 167.
[4] S. M. Hammond, A. A. Caudy, G. Hannon, *J. Nat. Rev. Genet.* **2001**, *2*, 110–119.
[5] S. M. Elbashir, J. Harborth, W. Lendeckel, A. Yalcin, K. Weber, T. Tuschl, *Nature* **2001**, *411*, 494–498.
[6] N. J. Caplen, *Expert Opin. Biol. Ther.* **2003**, *3*, 576–586.
[7] Y. Dorsett, T. Tuschl, *Nat. Rev. Drug Discov.* **2004**, *3*, 318–329.
[8] G. J. Hannon, J. J. Rossi, *Nature* **2004**, *431*, 371–378.
[9] V. Mittal, *Nat. Rev. Genet.* **2004**, *5*, 355–365.
[10] R. C. C. Ryther, A. S. Flynt, J. A. Phillips, J. G. Patton, *Gene Ther.* **2005**, *12*, 5–11.
[11] M. Sioud, *J. Mol. Biol.* **2005**, *348*, 1079–1090.
[12] L. Crombez, A. Charnet, M. C. Morris, G. Aldrian-Herrada, F. Heitz, G. Divita, *Biochem. Soc. Trans.* **2007**, *35*, 44–46.
[13] A. D. Judge, V. Sood, J. R. Shaw, D. Fang, K. Mc-Clintock, I. MacLachlan, *Nat. Biotechnol.* **2005**, *23*, 457–462.
[14] C. E. Thomas, A. Ehrhardt, M. A. Kay, *Nat. Rev. Genet.* **2003**, *4*, 346–358.
[15] N. Unnamalai, B. G. Kang, W. S. Lee, *FEBS Lett.* **2004**, *566*, 307–310.
[16] K. S. Suslick, M. W. Grinstaff, *Abs. Pap. Am. Chem. Soc.* **1994**, *207*, 57–INOR.
[17] M. W. Grinstaff, K. S. Suslick, *Proc. Natl. Acad. Sc. USA* **1991**, *88*, 7708–7710.
[18] K. S. Suslick, M. W. Grinstaff, K. A. Kolbeck, M. Wong, *Ultrason. Sonochem.* **1994**, *1*, S65–S68.
[19] K. S. Suslick, M. W. Grinstaff, *Abs. Pap. Am. Chem. Soc.* **1991**, *201*, 197–POLY.
[20] M. Wong, K. S. Suslick, *Abs. Pap. Am. Chem. Soc.* **1995**, *210*, 587–INOR.
[21] U. Angel (Shimanovich), D. Matas, S. Michaeli, A. Cavaco-Paulo, A. Gedanken, *Chem. Eur. J.* **2010**, *16*, 2108–2114.
[22] F. Kratz, I. Fichtner, U. Beyer, P. Schumacher, T. Roth, H. H. Fiebig, *Eur. J. Cancer.* **1997**, *33*, 784.
[23] C. Chevalier, A. Saulnier, Y. Benureau, D. Flchet, D. Delgrange, F. Colbre-Garapin, C. Wychowski, A. Martin, *Mol. Ther.* **2007**, *15*, 1452–1462.
[24] R. Prabhu, R. F. Garry, S. Dash, *Virol. J.* **2006**, *3*, 100.
[25] A. Gedanken, *Chem. Eur. J.* **2008**, *14*, 3840–3853.
[26] S. Avivi, Y. Nitzan, R. Dror, A. Gedanken, *JACS.* **2003**, *125*, 15712–15713.
[27] O. Grinberg, M. Hayun, B. Sredni, A. Gedanken, *Ultrason. Sonochem.* **2007**, 661–666.
[28] O. Grinberg, A. Gedanken, C. R. Patra, S. Patra, P. Mukherjee, D. Mukhopadhyay, *Acta Biomaterialia* **2009**, *5*, 3031–3037.
[29] U. Shimanovich, V. Volkov, D. Eliaz, A. Aizer, S. Michaeli, A. Gedanken, *Stabilizing Small* **2011**. *7*, 1068.
[30] U. Shimanovich, D. Eliaz, A. Aizer, I. Vayman, S. Micheli, Y. Shav-Tal, A. Gedanken, *ChemBioChem* **2011**, *12*, 1678–1681.
[31] M. E. C. D. R. Oliveira, G. Hungerford, M. D. Miguel, H. D. Burrows, *J. Mol. Struct.* **2001**, *563*, 443–447.
[32] T. Sacket, J. Wolff, *Anal. Biochem.* **1987**, *167*, 228–234.
[33] http://www.bitplane.com/(accessed July 2011).
[34] http://scion-image-software.fyxm.net/(accessed July 2011).
[35] http://flowcytometry.ualberta.ca/(accessed July 2011).